Propagation of nanosecond discharge in an air gap containing a water droplet: modelling and comparison with time-resolved images

Anthony Ouali, Lyes Sebih, Antoine Herrmann, Flavien Valensi, Ahmad Hamdan

Propagation of nanosecond discharge in an air gap containing a water droplet: modelling and comparison with time-resolved images

Anthony Ouali[1,2], Lyes Sebih[1], Antoine Herrmann[1], Flavien Valensi[2], and Ahmad Hamdan[1,*]

[1] Groupe de physique des plasmas, Département de Physique, Université de Montréal, 1375 Avenue Thérèse-Lavoie-Roux, Montréal, H2V 0B3, Québec, Canada

[2] Université de Toulouse, LAPLACE (Laboratoire Plasma et Conversion d'Energie) 118 route de Narbonne F-31062 Toulouse Cedex 9, France

*corresponding author. Email: ahmad.hamdan@umontreal.ca

Keywords: nanosecond discharge, dielectric liquid, streamer, fluid model, temporal resolved imaging.

ABSTRACT

Plasma-water interface is a complex medium, and the majority of the physical and chemical phenomena of interest are produced at the interface. Herein, we develop a 2D fluid model to study the ignition and propagation of streamer discharge in air gap with a droplet of deionized water lying on a Teflon surface. The droplet is considered as a perfect solid dielectric due to the fast propagation of streamer. The model consists of resolving Poisson's equation as well as the drift-diffusion equation for electrons, positive ions, and negative ions. The utilized transport coefficients are tabulated as a function of the reduced electric field. The photoionization is considered in the model thanks to Helmholtz equations. The results of the model are first compared with the experimental one, which is the emission of 1 ns-integrated ICCD images. Such a comparison allows a validation of the model. Then, the model is utilized to investigate the influence of the dielectric permittivity of the droplet as well as its wetting angle (contact angle between the droplet and the Teflon surface) on the properties of the discharge. In general, this simplified model is validated thanks to a comparison with experimental results as well as with other existing complex models. Therefore, it can be further developed to investigate other configurations and to determine some plasma properties at the interface not accessible experimentally.

1. INTRODUCTION

Streamer discharge is known to be a medium composed of highly reactive species (electrons, radicals, photons, etc.) coupled to extreme physical condition such as intense electric field (e.g. space charge field of ~150 kV/cm [1]), shock waves, and energetic electrons (5-10 eV [2]). Plasmas with such properties have shown interest for many applications, such as environmental remediation [3], material processing [4], medicine [5], and others [6]. It is also worth noting that streamer discharges are encountered in natural plasmas, e.g. lightnings [7].

In the context of applications, streamers are usually placed in contact with a surface that can be solid or liquid. In the case of liquid surface, many phenomena occur at the plasma-liquid interface, including evaporation, surface deformation, droplet ejection, charge accumulation, secondary electron emission, as well as sheath formation [8]. As most of the physical and chemical phenomena occur at the plasma–liquid interface, it is essential to further investigate the properties and dynamics of processes occurring in this region..

During the last decade, many research studies investigated the plasma–liquid interface by studying the discharge emission at the liquid surface, and patterns are usually observed. Depending on the experimental conditions, various patterns are observed, including discs, rings, dots, as well as a mixture of more than one pattern [9- 14]. As they are produced at the liquid surface, the emission patterns indicate the complex dynamics and, therefore, the mechanisms involved in the production and transport of reactive species.

The optimization of reactive species transport from the plasma to the liquid is one the main challenges in plasma–liquid research, according to the 2022 plasma roadmap [15]. It was suggested that such optimization must be conducted using systems with large surface-to-volume ratios.

Practically, there are many geometries that exhibit a large surface-to-volume ratio. However, from an experimental point of view, droplets (where surface-to-volume ratio is inversely proportional to the droplet's radius) remain the simplest geometry to realize and investigate.

Over the past few decades, plasma-droplet systems are investigated mainly in the context of lightning ignition [16], and material synthesis (interactions in plasma–(micro-)droplet systems, also known as plasma sprays or misty plasmas) [17]. In 2020, Oinuma *et al* [18] studied the transfer of OH radicals from a diffuse RF glow discharge (in He with 0.2% H2O) to a micrometre-size droplet of water that contains formate. They found that formate conversion is dominated by nearinterfacial reactions with OH radicals. More recently, Zhao *et al* [19] studied the propagation dynamics of single discharges produced in an air gap containing a millimetre-size suspended water droplet. The authors show that the discharge is initiated in the air gap between the anode and the droplet, then it propagates over the droplet. In 2023, Hamdan and Dorval [20] have also studied the spatio-temporal dynamics of a nanosecond discharge in air with a water droplet lying on a Teflon surface. The authors found that the discharge is ignited as streamer at the electrodes and reached the droplet within few nanoseconds. Then, after being propagated over the droplet, a transition to a spark (at high voltage condition) is observed. In a plasma-droplet system, the experimental determination of some fundamental plasma properties, such as electric field, species densities, etc., remains a challenge due to the fast spatio-temporal dynamics of the discharge. Therefore, modelling studies offer a unique opportunity to report such quantities. In this context, several models of plasma-surface (the surface of a droplet, particle, or bubble) interactions have

been developed to address the physical and chemical phenomena occurring at the interface [21,22]. For instance, Babaeva and Kushner [21] have studied the impact of inhomogeneities (particles or bubbles) present in the gap on the propagation and morphology of positive streamers. Since

particles and bubbles are considered as high- and low-density areas, respectively, the authors found that the particles induced streamer deflection, while the bubbles attracted the streamer. In another study [23], the authors investigated the impact of the dielectric permittivity on the propagation of positive streamer in an immersed bubble. They showed that low ratio of dielectric permittivity between liquid and bubble (e.g. 2/1) the discharge propagates axially inside the bubble, while it propagates along the interface at higher ratio (e.g. 80/2). More recently, Konina et al. [24] simulated the propagation of a negative and positive surface ionization wave at the surface of water droplet (diameter of 475 μm). The authors found that the positive ionization wave propagated close to the droplet-air interface, while the negative one initially propagates close to the interface but later detaches and propagates away from the interface due to the polarization of the droplet.

In the reported literature, it is rare to find experimental and modelling studies conducted under similar conditions, which is the goal of this study. Indeed, we develop a simplified 2D fluid model to simulate the ignition and propagation of a discharge in the air gap containing a water droplet lying on a Teflon surface. This same configuration is also investigated experimentally by acquiring 1 ns-integrated ICCD images. The model allows for the determination of fundamental discharge properties that cannot be obtained experimentally, such as spatio-temporal evolution of electron density, electric field, and space charge density. The experimental setup and the numerical model are described in Section 2 and 3 and, respectively, and the results are compared together in section 4.1. Discharge morphology and propagation velocity are presented in sections 4.2 and 4.3, respectively. The model is also utilized to study the influence of droplet's dielectric permittivity and wetting angle on the discharge dynamics (section 4.4).

2. EXPERIMENTAL SETUP

The experimental setup to produce single discharge in air with water droplet is detailed in ref. [20]. Therefore, only a brief description is presented here. The discharge is produced between copper electrodes using single pulses provided by negative polarity power source (NSP 120-20-N-500-TG-H; Eagle Harbor Technologies) at an amplitude of –11 kV and a pulse width of 300 ns. The electrodes are placed on a Teflon surface, as presented in Figure 1a. A (half-) droplet of deionized water is deposited at the Teflon surface. The droplet diameter is 4 mm and is centred between the electrodes that has a gap of 5 mm. A typical image of the streamer discharge, integrated over 50 discharges with a commercial camera (Fujifilm-x-s10 model), is presented in Figure 1b.

The negative high voltage was connected to the electrode at the left-hand side, while the electrode at the right-hand side was grounded (Figure 1a). The dynamic of the discharge emission was determined using an ICCD camera (PIMAX-4: 1024 EMB, Princeton Instruments) coupled with an optical lens. The camera is mounted in a way to capture a side view of the discharge. The synchronization between the camera and the high voltage pulse was achieved using a delay generator (Quantum Composers Plus 9518 Pulse Generator). A high-voltage probe (P6015A, ×1000; Tektronix) and a current probe (6585, 0.5 V/A; Pearson) were used to measure the voltage and current waveforms of the discharge, respectively. The waveforms were acquired using an oscilloscope (MSO54, 2 GHz, 6.25 GS/s; Tektronix). Current-voltage waveforms for a typical discharge are shown in Figure 1c, where a current peak of ~1.5 A is measured (further details on the electrical characteristics can be found in ref. [20]).

Streamer discharge captured with the ICCD camera required a post processing of all the images of multiple different discharges to establish a temporal evolution. The time associated with each image is determined using the electrical signature of the streamer discharge and the synchronization signal sent by the delay generator.

The nature of the surface where the droplet is deposited can significantly change the behavior of the droplet due to the contact angle. In the case of Teflon surface and deionized water droplet (electrical conductivity of ~3 μS/cm), the shape is almost a hemisphere. The influence of the shape of the droplet is discussed in Section 4.2, using numerical results.

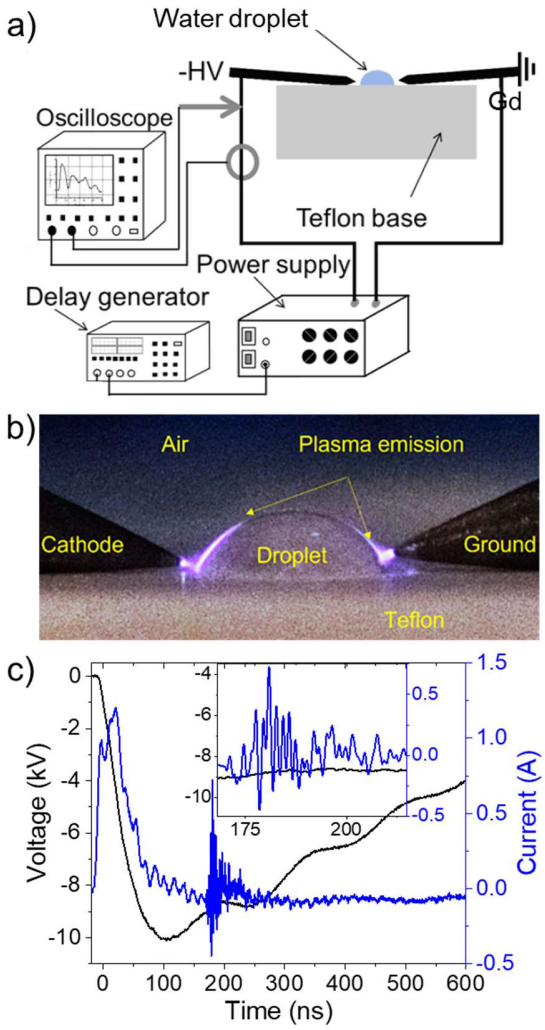

Figure 1: *a) Scheme of the experimental setup to produce streamer discharge in air gap with a droplet of deionized water. b) Typical image of a streamer discharge integrated over 50 discharges with a commercial camera. c) Current-voltage waveforms for a typical discharge conducted at –11 kV and 300 ns of voltage amplitude and pulse width, respectively.*

3. NUMERICAL MODEL

3.1. Fluid model

In this study, a fluid model based on the drift-diffusion approximation is used to determine the mean velocity of the charged particles, namely electrons, positive ions, and negative ions. To close the system of equations, we assume that the transport and reaction coefficients only depend on the reduced electric field (E/N), with E the norm of the electric field, determined using Poisson's equation, and N the density of the gas. The system of hydrodynamic equations can be written as follows:

$$\frac{\partial n_i}{\partial t} + \vec{\nabla}.\left(n_i \mu_i \vec{E} - D_i \vec{\nabla} n_i\right) = G_i \qquad (1)$$

$$\vec{\nabla}.\left(\epsilon_0 \epsilon_r \vec{\nabla}\phi\right) = -\rho = -e\left(n_p - n_e - n_n\right) - \sigma_s \delta_s \qquad (2)$$

$$\vec{E} = -\vec{\nabla}\phi \qquad (3)$$

where n_i is the density (m^{-3}) of the i-species (i represents the electron (e), positive ion (p) or negative ion (n)), μ_i ($m^2.V^{-1}.s^{-1}$) and D_i ($m^2.s^{-1}$) are respectively the mobility and the diffusion coefficients of the i-species, G_i ($m^{-3}.s^{-1}$) is the source term of the i-species, ϵ_0 is the vacuum dielectric permittivity constant, ϵ_r is the dielectric constant of the medium, ϕ (V) is the electrical potential, e (C) is the elementary charge, σ_s ($C.m^{-2}$) is the charge of the dielectric surface, δ_s (m^{-1}) is the Kronecker delta and represents the position of the dielectric surface, and $\vec{E}$ ($V.m^{-1}$) is the vector electric field.

The flux of the i-species is defined as follow:

$$\vec{\Gamma}_i = n_i \mu_i \vec{E} - D_i \vec{\nabla} n_i \qquad (4)$$

As we aim to develop a simplified model, it does not consider all the different chemical reactions that can occur in atmospheric pressure air plasma. Instead, global coefficients are used: α (m^{-1}) represents the ionization, η (m^{-1}) represents the attachment, β_{ep} ($m^3.s^{-1}$) represents the electron-

ion recombination, and β_{pn} ($m^3.s^{-1}$) represents the recombination between positive and negative ions. The expression of all those parameters can be found in [25]. The source terms for electrons, positive ions, and negative ions can be respectively written as follow:

$$G_e = S_e - \eta n_e \mu_e \left|\vec{E}\right| - \beta_{ep} n_p n_e + S_{ph} \quad (5)$$

$$G_p = S_e - \beta_{ep} n_p n_e - \beta_{pn} n_p n_n + S_{ph} \quad (6)$$

$$G_n = \eta n_e \mu_e \left|\vec{E}\right| - \beta_{pn} n_p n_n \quad (7)$$

where S_{ph} is photoionization source term (developed in Section 3.2) and S_e is the electron impact ionization source term that can be expressed as $S_e = \alpha n_e \mu_e \left|\vec{E}\right|$; it represents electrons generated by the collision between energetic electrons and heavy particles. This expression needs special attention, as it can lead to non-physical ionization particularly in the region where n_e is large and $\mu_e \left|\vec{E}\right|$ is small, e.g. the region right behind the head of the positive streamer. If considered, those non-realistic electrons can then diffuse to the head of the streamer and generate electronic avalanches. To be considered correctly, Teunissen [26] suggested to replace the norm of the drift flux $\left|\vec{\Gamma}^{drift}\right| = n_e \mu_e \left|\vec{E}\right|$ by the minimum between the norm of the drift flux and the norm of the flux $\left|\vec{\Gamma}\right|$, i.e. Eq. (4). The source terms are rewritten as follow:

$$G_e = (\alpha - \eta) \min\left\{\left|\vec{\Gamma}^{drift}\right|, \left|\vec{\Gamma}\right|\right\} - \beta_{ep} n_p n_e + S_{ph} \quad (8)$$

$$G_p = \alpha \min\left\{\left|\vec{\Gamma}^{drift}\right|, \left|\vec{\Gamma}\right|\right\} - \beta_{ep} n_p n_e - \beta_{pn} n_p n_n + S_{ph} \quad (9)$$

$$G_n = \eta \min\left\{\left|\vec{\Gamma}^{drift}\right|, \left|\vec{\Gamma}\right|\right\} - \beta_{pn} n_p n_n \quad (10)$$

3.2. Photoionization

The mechanism of photoionization is well known in discharges, and it becomes important when energetic photons (e.g. UV) are emitted in the medium. In the case of discharges in dry air, i.e.

N_2–O_2 gas mixture, excited N_2 molecules can emit UV photons (~12 eV) that can photoionize O_2 molecules (ionization energy of ~12 eV) [27]. To consider this phenomenon, different models were used. A first model assumes a uniform background source term. Although this model performed well in simplified configurations, it becomes invalid in a relatively complex configuration [28], such the one studied here. Therefore, a second more complete model was introduced by Zhelezniak et al. [29] and is well described by Celestin [30]. This model consists of computing S_{ph} at a position $\vec{r}$ thanks to the following integral:

$$S_{ph}(\vec{r}) = \iiint \frac{I(\vec{r}\prime)g(|\vec{r}-\vec{r}\prime|)}{4\pi|\vec{r}-\vec{r}\prime|} dV' \qquad (11)$$

where $I(\vec{r}')$ is the production rate of photons that generate an electron at the position $\vec{r}'$. This function is proportional to the density of radiative excited species or, on first approximation, proportional to the ionization source term. The function $g(|\vec{r}-\vec{r}'|)$ depends on the partial pressure of the photoionized species (here is that of oxygen (p_{O_2})) and $|\vec{r}-\vec{r}'|$; p_{O_2}~150 Torr at atmospheric pressure. The integral (Eq. 11) needs to be computed at every $\vec{r}$ of the domain for every time step, which makes its computational cost very high. To reduce this cost, a third model was introduced by Luque et al. [31], and it consists to approximate the function $g(|\vec{r}-\vec{r}'|)$ as a sum of multiple exponential functions. The photoionization source term is then written as a sum where each coefficient satisfies a Helmholtz equation:

$$\nabla^2 S_{ph}^k(\vec{r}) - (\lambda_k p_{O_2})^2 S_{ph}^k(\vec{r}) = -A_k p_{O_2}^2 I(\vec{r}) \qquad (12)$$

where λ_k and A_k are fit parameters.

Table 1: *The fit parameters utilized to compute the photoionization source term*

$\boldsymbol{k}$	$\boldsymbol{\lambda}\ [\boldsymbol{cm^{-1}.Torr^{-2}}]$	$\boldsymbol{A}\ [\boldsymbol{cm^{-2}.Torr^{-2}}]$
1	0.0553	1.986×10^{-4}
2	0.1460	0.0051
3	0.89	0.4886

In this study, we use the three-exponential fit, so we must solve three Helmholtz equations. The computational cost is still less than the integral model because of the possibility to use the same solver for the Poisson's equation (Eq. 2).

3.3. Poisson's equation

The starting point of the streamer model is the resolution of Poisson's equation. The electric field is a key element in a streamer model because all transport parameters and source terms have a strong non-linear dependence on it. Therefore, a good accuracy on the electric field is needed at each time step. In the following section, we introduce the Ghost Fluid Method (GFM) applied to Poisson's equation to calculate accurately the potential and the electric field.

In the presence of an interface separating two dielectric media with dielectric permittivity of $\epsilon_1$and ϵ_2, the normal component of the electric field is discontinuous, and it can be calculated using the following equation:

$$(\epsilon_2\vec{E}_2 - \epsilon_1\vec{E}_1).\vec{n}_{12} = \sigma_s \qquad (13)$$

where $\vec{n}_{12}$ is the unit vector normal to the interface and σ_s is the surface charge of the interface. The role of the GFM is to modify the discretization of Eq. 2 to consider this discontinuity at the exact position of the interface. This method is described in detail by Dubinova et al. [32]. The

new discretization keeps the sparse property of the matrix representative of the linear system, and the computational cost is not modified.

At the surface of the electrodes and the surface of water droplet different phenomena can occur. The first one is secondary emission of electron due to ion bombardment. A coefficient, γ, is introduced and generally fixed to 0.1 to consider electrons generated at the surface of electrodes. At the surface of water, secondary emission is known to be small. However, photo-electron emission takes an important role. Therefore, a generalized $\gamma = 0.1$ is considered [33].

The surface charge density is calculated using the flux of every charged particle who comes from the gas to the dielectric interface. The temporal evolution of the surface charge density can be represented as follows:

$$\frac{\partial \sigma_s}{\partial t} = -e\left[\left((1+\gamma)\vec{\Gamma}_p - \vec{\Gamma}_n - \vec{\Gamma}_e\right).\vec{n}\right] \qquad (14)$$

with $\vec{n}$ is a unit vector perpendicular to the dielectric surface and pointing to the gas. Eq. 14 is true only when the scalar product of $\vec{\Gamma}$ by $\vec{n}$ is negative.

To solve the system, we use a direct solver based on the LU factorisation [34]. The LU factorisation permit to rewrite a matrix A as the product of two matrices L and U. L is block lower triangular and U is block upper triangular. Python offers a large panel of fundamental algorithms for scientific computing such as SciPy [35]. This module, written in C, Fortran, and C++, provides optimized algorithms to solve linear system. In addition to accelerate the solving time, the decomposition of A into L and U matrices is an interesting property because LU factorisation remains the same when A is unchanged. In our case, this property can be fully exploited because the matrix does not depend on time but only on the spatial structure of the

system. Thereby, the matrix factorized at the beginning of the code is exploited at each time step thanks to SciPy functions.

3.4. Flux computation

Once the electric field is computed, all the source terms can be calculated. The final part is to discretize spatially and temporally the continuity equation for each species. We use in this study the Finite Volume Method (FVM) which permits, by construction, to conserve the computed quantity. Another widely used method is the finite-element method (FEM). The advantage of this latter is its capacity to capture nonuniform geometries. However, this method is not conservative. Therefore, to consider the physics of the problem (e.g. conservation of electron density in the domain), we choose to solve the problem with FVM.

3.4.1. Spatial discretization

The FVM consists of integration the conservation equation over a control volume, i.e. a cell. Using the divergence theorem, the volume integral is converted to a surface integral on cell's surfaces. This method needs to be coupled to a numerical scheme. Three categories are usually used: Upwind [36], flux limiter [37], and Scharfetter-Gummel [38]. Upwind scheme is first order and may introduce numerical diffusion. The two last methods are second order and usually lead to similar results [30]. In this study, we choose to use Scharfetter-Gummel scheme, because it provides exact solution between two points of the mesh of the 1D steady drift-diffusion equation. This scheme assumes a constant electric field in each cell. A more accurate version assumes a linear variation of the electric field between cells but adds a parameter that must be adjusted to introduce no oscillation [39]. To keep it as simplified as possible, the first stable version of the Scharfetter-Gummel was used.

To discretize Eq. 2, using the numerical method presented above, a mesh is needed. Because of the geometry, the different length scales present in a streamer propagation, and the presence of different dielectrics medias, the steps must be very short (0.8 μm). If a uniform grid is used, the computational cost is too high (one calculation may take more than 1 week). To optimize the calculation time, adaptative mesh refinement methods may be used to resolve similar problems [40]–[42]. However, to be efficient, those methods need to be coupled with parallelization strategies. In our case, because Python is not as efficient as C for parallelization, a non-uniform grid is utilized in the calculation. With such a grid, it is feasible to increase the number of points in critical areas, such as dielectric surface, high electric field region, and cathode sheath, and to reduce the number of points in region of less interest (far from the streamer path).

3.4.2. Temporal discretization

In accordance with the second order spatial discretization, we used a second order Runge-Kutta method. Streamer discharge employs processes that occur at different timescales, and it is important that every process must correctly be captured by the code. Limits on the time step are thus introduced. First, the time step must be shorter than the typical characteristic time of diffusion and advection, defined as [39]:

$$dt = \min\left\{\frac{0.6\,dx}{max\{\mu_e|\vec{E}|\}}, \frac{0.6\,dx^2}{D_e}\right\} \quad (15)$$

Poisson's equation also introduces a limit on the time step. When an electric field is applied, charges move to screen it. This movement takes some time and must be correctly modelized particularly when Poisson's equation and conservation equations are not coupled, which is the case here. This time scale that needs to be considered is well known as dielectric relaxation time.

In practice, this time scale can be very short (10 times shorter than the advection time scale). To avoid a computational time too long by using this time restriction, we used the method developed by Teunissen et al. [26]. It consists of limiting the total electron flux along a j-axis, defined by:

$$\left|\Gamma_j\right| \leq \frac{\epsilon_0}{e\Delta t} \max\left\{\left|E_j\right|, \frac{D_e\left|\partial_j n_e\right|}{\mu_e n_e}\right\} \quad (16)$$

If equation (16) is not satisfied, the new flux along j-axis is then considered as:

$$\Gamma_j = sign\left(\Gamma_j\right) \frac{\epsilon_0}{e\Delta t} \max\left\{\left|E_j\right|, \frac{D_e\left|\partial_j n_e\right|}{\mu_e n_e}\right\} \quad (17)$$

where $sign\left(\Gamma_j\right)$ is defined as:

$$sign(\Gamma_j) = \begin{cases} 1 \; if \; \Gamma_j > 0 \\ -1 \; if \; \Gamma_j \leq 0 \end{cases} \quad (18)$$

3.5. Numerical domain

The numerical domain is presented in Figure 2. The droplet is represented by a hemisphere. The center of the circle can be adjusted to approach the real shape of the droplet. In our case the droplet has a contact length with Teflon, d_{cl}, of 4 mm, and the height, d_h, is 1.2 mm. The shape of the electrodes plays an important role in the spatial distribution of the electric field (the geometric electric field), particularly in the absence of discharge. Although this geometric electric field defines the value of the breakdown voltage and the initial shape of the streamer, its influence becomes insignificant as soon as the space charge density becomes high enough to deform the geometric electric field. Therefore, to simplify the simulation, we choose not to consider a pin electrode (as in the experimental) but rather a rod with quarter circle head, as shown in Figure 2. The thickness of both electrodes is represented by d_e and fixed to 0.3 mm. The gap, d_g, is set to 5 mm.

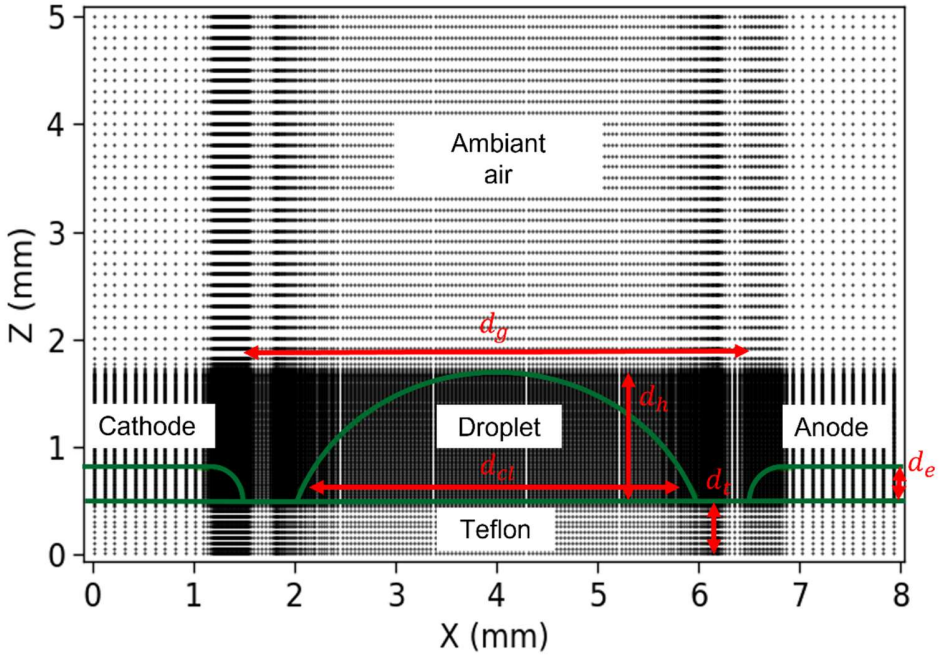

Figure 2: *Numerical domain where the simulation is conducted. The grid is composed of 1550×1030 points. The green lines indicate the electrodes, the Teflon surface, and the droplet surface.*

The numerical domain is discretized on a grid of 1550×1030.

Along the X-axis:

- $\Delta x = 1\ \mu m$ at the electrode surface and the dielectric surface
- $\Delta x = 10\ \mu m$ in the gap between the electrode and the water droplet

Along the Z-axis:

- $\Delta z = 10\ \mu m$ in the Teflon
- $\Delta z = 2\ \mu m$ at the Teflon's surface
- $\Delta z = 1\ \mu m$ at the top of the droplet
- $\Delta z = 20\ \mu m$ at the end of the domain

3.6. Initial conditions and boundary conditions

To initialize the discharge, we added two gaussian distributions of electrons and ions with amplitude $10^{18}\ m^{-3}$ close to the electrode heads; the entire air domain is filled with a uniform electrons and ions with density of $10^{8}\ m^{-3}$. Negative ions are set to zeros in all the domain.

In presence of a dielectric surface together with electrons, positive ions, and negative ions, the flux of each species must satisfy the following conditions:

$$\begin{cases} \vec{\Gamma}_e.\vec{n} = \ sign(\vec{E}.\vec{n})\mu_e n_e \vec{E} - \big(1 - sign(\vec{E}.\vec{n})\big)\gamma\vec{\Gamma}_p.\vec{n} \\ \vec{\Gamma}_p.\vec{n} = \big(1 - sign(\vec{E}.\vec{n})\big)\mu_p n_p \vec{E} \\ \vec{\Gamma}_n.\vec{n} = \ sign(\vec{E}.\vec{n})\mu_n n_n \vec{E} \end{cases} \tag{19}$$

with $\vec{n}$ is unit vector perpendicular to the dielectric surface and pointing to the gas.

For electrodes surface, Table 2 summarizes the boundary conditions.

Table 2: *Boundary conditions at the electrode surfaces.*

	Anode	Cathode
n_e	$\vec{\nabla} n_e.\vec{n}^* = 0$	$\vec{\Gamma}_e.\vec{n} = \ -(1-\alpha_s)\gamma\vec{\Gamma}_p.\vec{n}$
n_p	0	$\vec{\nabla} n_p.\vec{n} = 0$
n_n	$\vec{\nabla} n_n.\vec{n} = 0$	0

* $\vec{n}$ is the unit vector perpendicular to the electrode surface and pointing to the gas.

4. RESULTS AND DISCUSSION

During a streamer discharge, electrons and ions are accelerated by the electric field and gain kinetic energy. Therefore, a complex chemistry can be achieved in this kind of plasma. Collisions between electrons and neutral species can produce ionization, excitation, and deexcitation. Therefore, photons at different wavelengths are emitted in the discharge.

Experimentally, the spatial-temporal evolution of the emitted photons that have wavelengths between 200 nm and 800 nm in the gap is obtained by the ICCD camera. This emission is compared to the source term S_e computed by the model; such comparison is utilized to validate the model [43]. The numerical model allows a more detailed characterisation of the streamer discharge by reporting data not accessible experimentally, such as spatial and temporal evolution of the electric field, electron density, and space charge density.

4.1. Model validation

4.1.1 Light emission and numerical results

Here, the aim is to validate the model by comparing the 1ns-integrated images with the model outputs. Among the many outputs of the model, the evolution of source term S_e can be compared to the ICCD images [43]. Indeed, this source term represents the number of electrons generated thanks to collision between energetic electrons and the particles in the medium. Considering that these electrons have enough energy to ionize, they have enough energy to excite molecules and atoms in the gas.

As detailed in Section 3.5, the experiment is conducted with a gap of 5 mm and voltage magnitude of 11 kV. The shape of the water droplet ($\epsilon_r = 80$) is a truncated circle of radius adjusted to consider a contact-length of 4 mm with the Teflon ($\epsilon_r = 2.1$). The droplet's height d_h (c.f Figure 2) is 1.2 mm.

Figure 3 compares the spatial-temporal evolution of S_e, predicted by the model, and the light emission captured by the ICCD camera. It is worth noting here that the camera integration time was 1 ns, and the model results are instantaneous. In general, the streamer dynamic predicted by the model is in good agreements with the experimental dynamics. Indeed, after an ignition of two streamers at the anode and cathode, they rapidly propagate at the Teflon surface and reach the droplet. Then, negative and positive streamers simultaneously propagate at the droplet-air interface with different velocities. The streamers meet each other at the droplet top after ~10 ns, and this is in great agreement with the experimental ICCD images. At this stage, it is fair to assume that the numerical model is validated and, therefore, it can be further exploited to address some parameters not accessible experimentally.

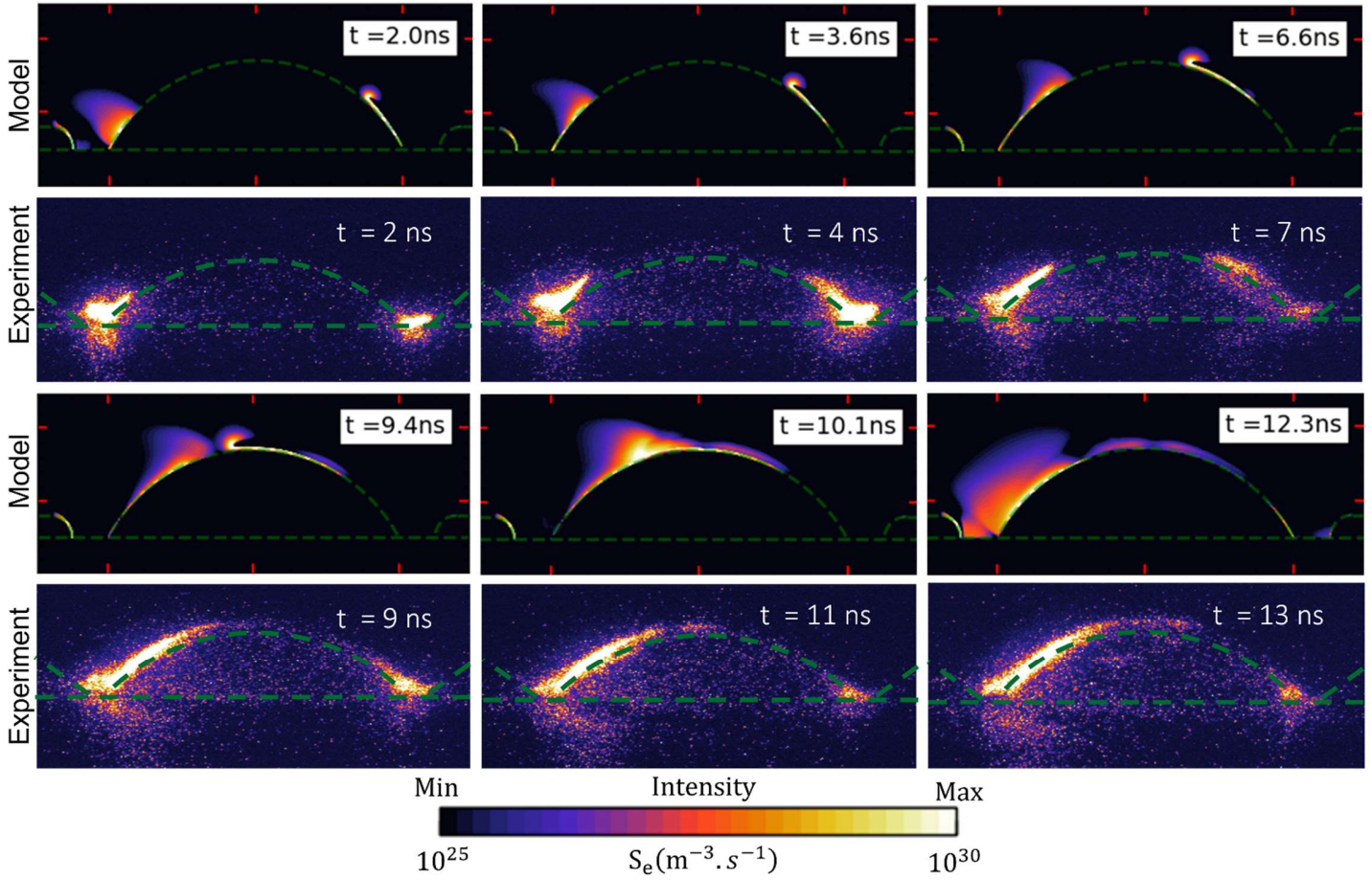

Figure 3: *Comparison between the time-evolution of S_e predicted by the model and the time-evolution of the emission (1 ns-integrated images) of the discharge in air gap with a droplet of deionized water. The cathode is on the left, the anode is on the right, and the applied voltage is 11kV.*

4.1.2 Streamers morphology

Streamer dynamic is strongly dependent on the spatial distribution of the electric field. The presence of the droplet and the Teflon surface strongly modifies the electric field distribution in the gap due to their dielectric permittivity constants. Therefore, it is crucial to report the temporal evolution of the electric field, as well as other quantities, such as electron density and space charge density.

When the voltage is applied, the negative streamer starts its propagation due to the initial spot of electrons near the cathode. For the positive streamer, its propagation is delayed by a period needed to generate enough space charge to deform the applied electric field. However, in less then 0.6 ns (Figure 4a), both streamers reach the surface of the droplet.

Between the surface of the droplet and the positive streamer, a sheath is formed due to the low mobility of positive ions as compared to that of electrons. Initially, positive ions are accelerated to the surface, whereas negative ions and electrons are accelerated towards the anode. Due to the strong non-neutrality, as illustrated in Figure 4b, an electric field is generated, and a sheath is formed. At this moment, the electric field at the head of the negative streamer is ~50 $kV.cm^{-1}$. As for the positive streamer, the electric field is ~900 and 250 $kV.cm^{-1}$ in the sheath and at the streamer's head, respectively. As expected, the electric field at the head of negative streamer is lower than that of positive streamer. This property is due to the space distribution of charged particle in each streamer (Figure 4b). Indeed, in positive streamer, positive ions can be supposed motionless, while in negative streamer, electrons diffuse rapidly resulting in a larger streamer head and, thus, a lower electric field; this property has been also reported by Zhang et al. [44].

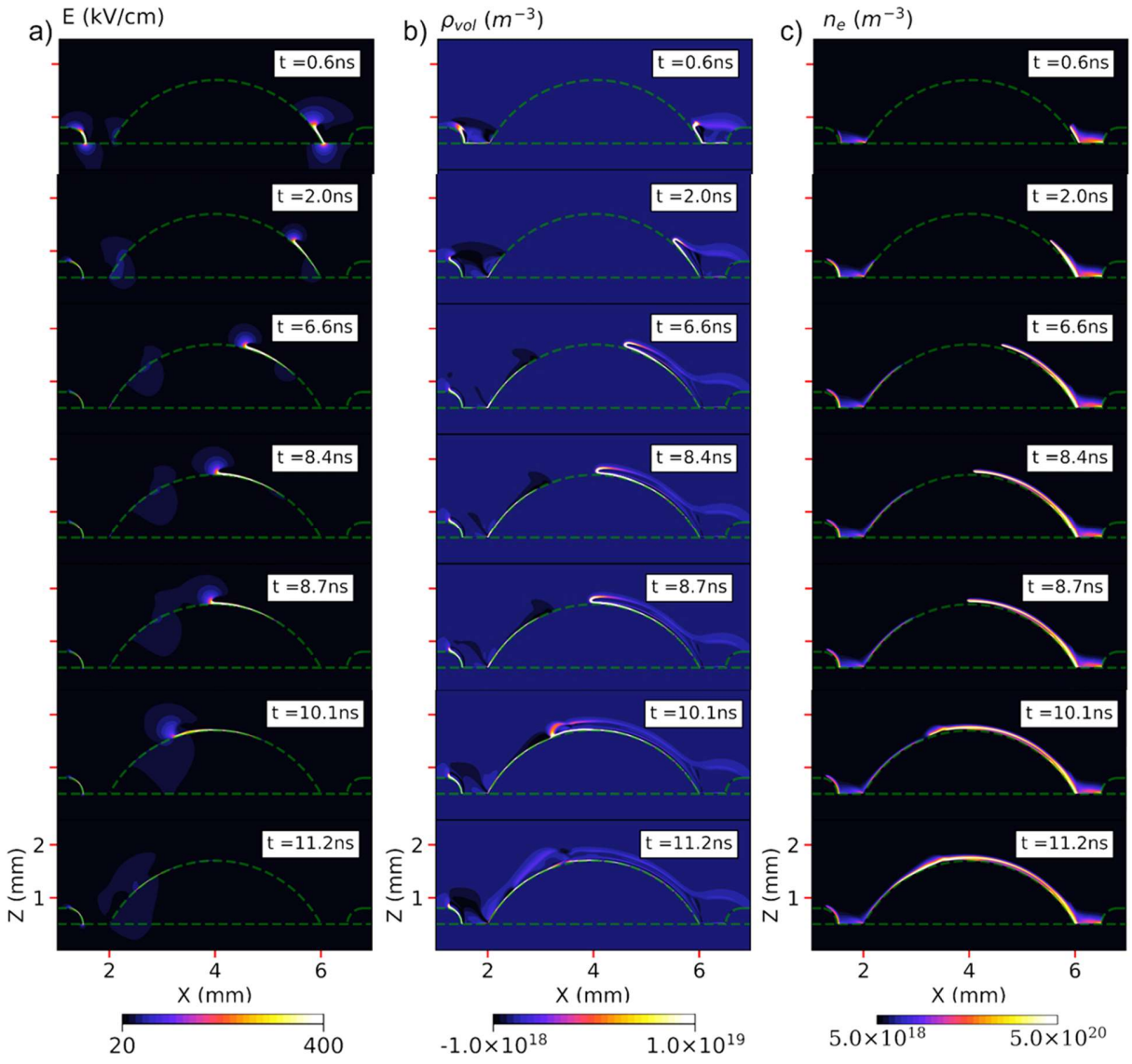

Figure 4: *Temporal evolution of a) the electric field, b) the space charge density, and c) the electron density of a discharge propagating in air gap with a droplet of deionized water.*

The second phase of the dynamic is the propagation of both streamers on the droplet surface until their contact at t = 10.1 ns. The negative streamer, easily identifiable thanks to the distribution of space charge density presented in Figure 4b, propagates glued to the dielectric surface. In fact, the sheath, formed by the presence of electrons on the dielectric surface, is immediately neutralized thanks to the high electron mobility. The electric field at the head of the negative streamer remains

around 50 kV.cm^{-1} during all its propagation period. In the case of positive streamer, the sheath dynamic is strongly correlated with the low ion mobility. When the number of positive ions becomes sufficient to repel positive species and attract electrons, the medium is slowly neutralised (Figure 4b), and the sheath slides with the positive streamer on the droplet, as presented in Figure 4a. The electric field in the head of the positive streamer slowly decreases during its propagation on the droplet surface to reach approximately 180 kV.cm^{-1} just before the contact between both streamers. The maximum of electric field in the sheath of the positive streamer also decreases to 740 kV.cm^{-1} at t = 10.1 ns.

After the contact between the positive and negative streamers, a conductive channel is formed at ~11 ns, as presented in Figures 4b and 4c. Figure 4c shows the distribution of n_e at different periods. At t = 0.6 ns, electron density in the head of positive streamer is $3 \times 10^{20}\ m^{-3}$ and is less than that in the head of the negative streamer by one order of magnitude. At t = 11 ns, the highest n_e in the conductive channel is around $10^{21}\ m^{-3}$.

The positive and negative streamers connect each other at the droplet in a point shifted towards the cathode. This fact is due to their different propagation velocities (detailed in next section). Finally, as the conductive channel is formed, the electric field is reduced significantly due to charge neutralization, but it remains larger than the breakdown electric field in air (30 kV.cm^{-1}). This property can lead to the formation of a spark discharge thanks to high ionization rate [45].

Interestingly, we notice a bump in the conductive channel, as shown in Figure 4c (at 10.1 and 11.2 ns). In fact, this bump is formed at 9.8 ns and can be explained by the electric field distribution. Indeed, initially, the electric field enhancement is produced at the surface of the droplet near the Teflon surface (275 kV.cm^{-1}). However, the electric field on the top of the droplet is lower than that in the gap (~1.1 vs ~80 kV.cm^{-1}). During the propagation of both streamers, the spatial distribution of the electric field is strongly modified, and the area of low electric field is shifted

436 with time. At t = 10 ns, electric field in this area is ~38 kV.cm^{-1}, while it is ~50 kV.cm^{-1} at the head
437 of the negative streamer. Therefore, due to a lower ionization rate in this area, it is bypassed by
438 both streamers producing thus a bump (or a bridge-like channel).
439 The numerical results also put forward the formation of a cathode sheath, as illustrated in Figure
440 4a (at 0.6 ns), where an electric field of ~700 kV.cm^{-1} is measured. As time goes on, its thickness
441 decreases significantly, while covering the head of the cathode. At t = 10 ns, the magnitude of the
442 electric field decreases to ~500 kV.cm^{-1}. After the creation of the conductive channel, the value of
443 the electric field in the cathode sheath increases. This is due to the non-consideration of the
444 variation of the voltage seen by the gas. Experimentally, when streamers propagate, a current is
445 measured and a drop in the gas voltage is observed [21]. To correctly simulate this phase, a
446 retroaction of the current on the applied voltage is needed.
447
448 **4.1.3 Propagation velocity of the streamers**
449 To determine the position of the positive streamer, a map of S_e is saved every 2000 iterations. The
450 coordinates X and Z of the maximum of S_e are saved, and the temporal evolution is fitted with a
451 polynomial function. Then, the speed is determined using the derivative of this function. For the
452 negative streamer, the maximum of S_e is also utilized. However, just before the contact between
453 both streamers, spatial distribution of S_e is utilized to determine the position of the negative
454 streamer's head.
455 Figure 5 shows the temporal evolution of streamers velocities, and it can be decomposed in four
456 regions (I-IV). In region (I), positive and negative streamers propagate on the Teflon surface and
457 reach the droplet surface. The negative streamer reaches the droplet first, which is consistent with
458 the experimental results. In fact, negative streamer needs a lower electric field to propagate due to
459 the high mobility of electrons. However, positive streamer, during its propagation, is faster than

460 the negative one (~0.7 vs 0.2 mm/ns) due to the high electric field. When the positive streamer
461 reaches the droplet, its velocity decreases significantly (to ~0.2 mm/ns). This decrease can be
462 related to the spatial redistribution of the electric field limited by the mobility of positive ions.
463 In region (II), both streamers have reached the droplet and propagate on its surface mainly along
464 the Z axis. Both streamers propagate at the same velocity (~0.2 mm/ns). In region (III) at t > 3.5
465 ns, both streamers have crossed the first quarter of the droplet and the velocity of the positive
466 streamer increases from ~0.2 to 0.3 mm/ns. This increase is due to the electrons generated at the
467 front of negative streamer and producing electron avalanche at the head of the positive streamer.
468 For the negative streamer, its speed remains around 0.1-0.2 mm/ns.

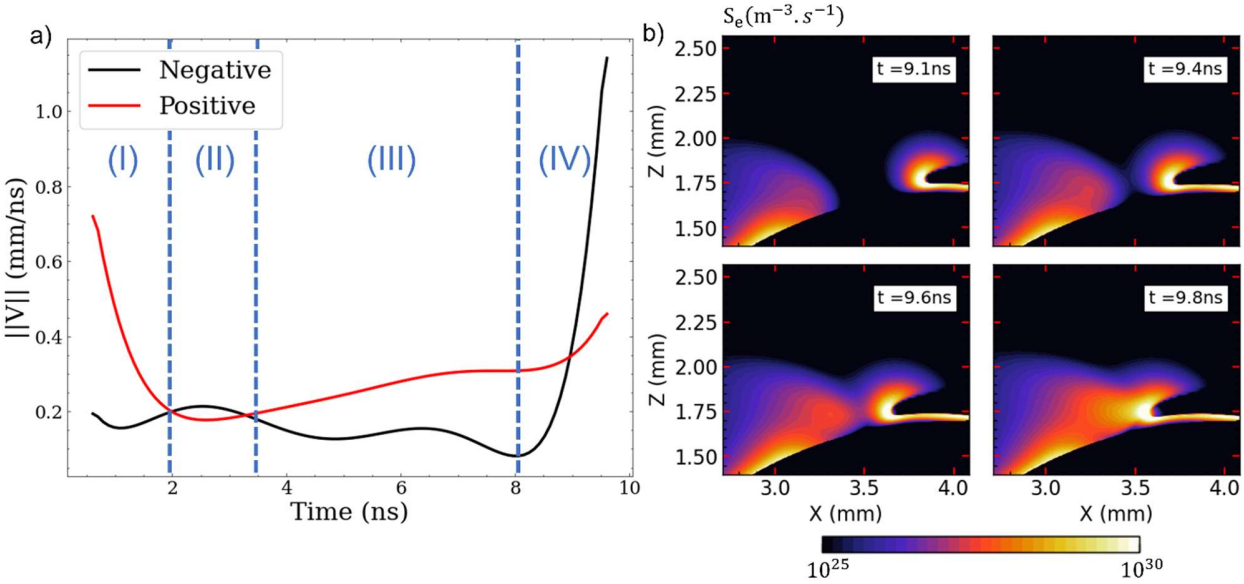

469

470 ***Figure 5:*** *a) Time-evolution of the propagation velocities of positive and negative streamers*
471 *propagating in the air gap with a droplet of deionized water. b) Time-evolution of S_e in the*
472 *period of region IV in a) that corresponds to the contact between the negative (at left) and*
473 *positive (at right) streamers.*
474

475 Just before the contact between both streamers (region IV), the velocity of the negative streamer
476 increases significantly from ~0.1 to 1.1 mm/ns. The period when the heads of positive and negative
477 streamers approach each other is shown in Figure 5. It is interestingly to notice that the negative

streamer is attracted be the positive one and peeled from the droplet surface. This behavior is due to the difference of mobility between heavy species and electrons and, thus, to local electric field distribution.

4.2 Influence of dielectric permittivity

The dielectric permittivity of the droplet is an important parameter the can significantly influences the ignition and propagation of the discharge due to the modification of the distribution of the electric field. To clearly highlights this influence, we conducted calculation for droplets that have different dielectric permittivity, namely 8, 24, 41, and 80.

Figure 6 shows the temporal evolution of n_e when the discharge propagates on the droplet's surface. The selected images demonstrate that the dielectric permittivity influences the propagation speed of positive and negative streamers as well as the electron density in the conductive channel. The propagation paths of the streamers will be discussed later, but it is of interest to highlight here that the behavior of the contact point between positive and negative streamers also depends on the permittivity of the droplet. In fact, the increase of ε_r displaces the contact point to the left, i.e. it approaches the cathode. This finding can be related to the propagation velocity of the streamers.

On the other hand, the development of the conductive channel depends on ε_r. For instance, it is developed within 12.3 ns at $\varepsilon_r = 80$, while at $\varepsilon_r = 8$ it is developed at 21.2 ns. Also, the simulation clearly shows that the highest electron density in the conductive channel is obtained with high-ε_r condition. For instance, at $\varepsilon_r = 80$ and 8, we measure 9×10^{20} and $2.5 \times 10^{20}\ m^{-3}$, respectively.

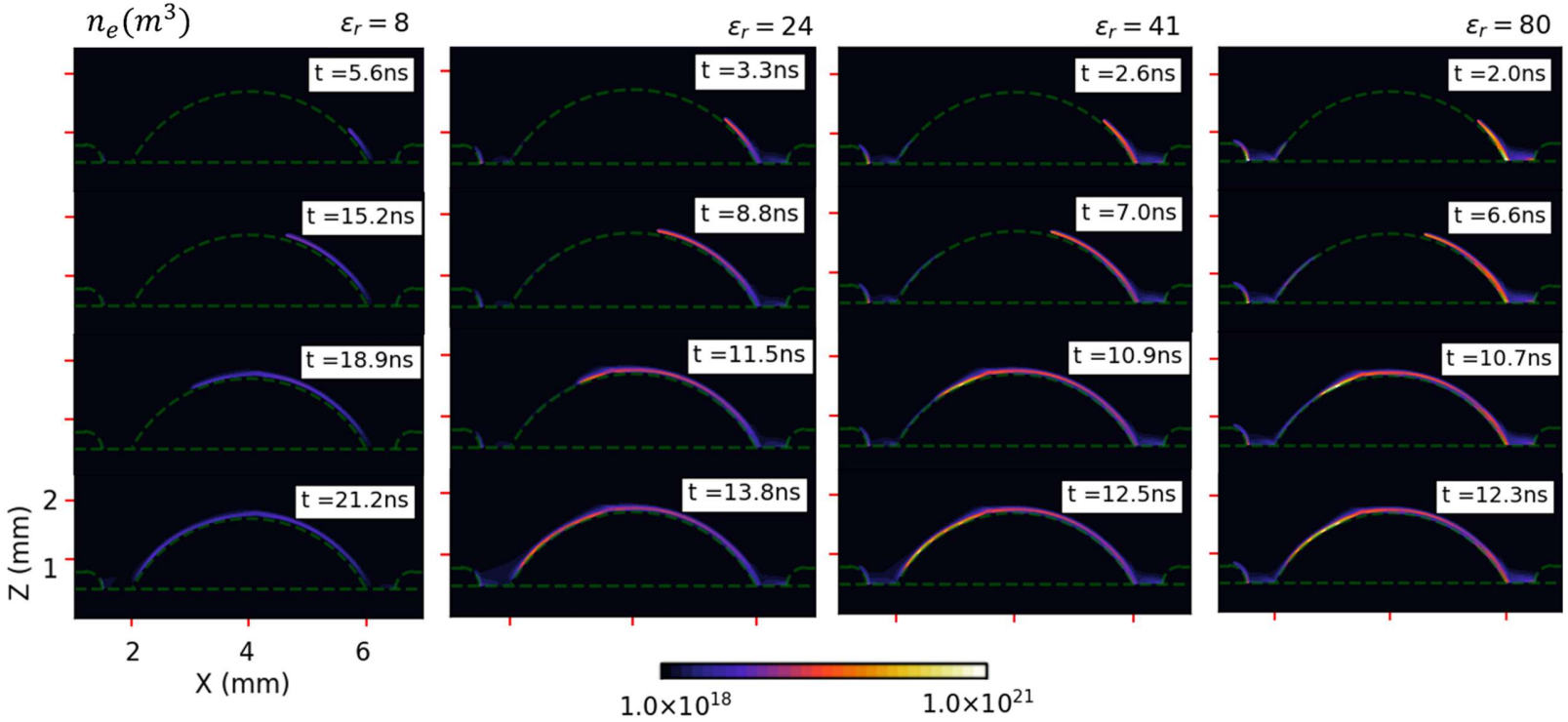

Figure 6: *Time evolution of electron density for streamer discharges propagating in air gap with a droplet that has different dielectric permittivity.*

503 Figure 7 represents the positions (X and Z) of both negative and positive streamers that propagate
504 in the gap with a droplet at different dielectric permittivity. These profiles clearly show different
505 regions during propagation. In the case of negative streamer, the propagation along Z exhibits two
506 trends, one slow and one fast. The growth rate depends on the permittivity of the droplet and is
507 higher at high ε_r; this is true in both slow and fast regions. The transition time from slow to fast
508 also depends on ε_r. For instance, it occurs at ~15 ns in the case of $\varepsilon_r = 8$, while it occurs at ~8.5 ns
509 in the case of $\varepsilon_r = 80$. The same trend is observed for the time evolution of X. The major difference
510 than can be highlighted is that the growth along X is faster than that along Z. The positive streamer
511 exhibits an opposite behavior than that of the negative one. Indeed, the slightly fast region is
512 observed initially, during the first few nanoseconds. Here also, the fastest propagation is observed
513 in the case of the high ε_r. A decrease region along the Z axis is highlighted for the positive streamer,
514 and it is due to the cross of the middle of the droplet by the positive streamer. These propagation
515 profiles can be well explained by the magnitude and distribution of the electric field. Indeed, the
516 electric field is highly sensitive to the ratio between the dielectric permittivity of the droplet and
517 of the medium. When this ratio increases, electric field in the air increases and leads to a faster
518 propagation on the dielectric due to higher ionisation rate.

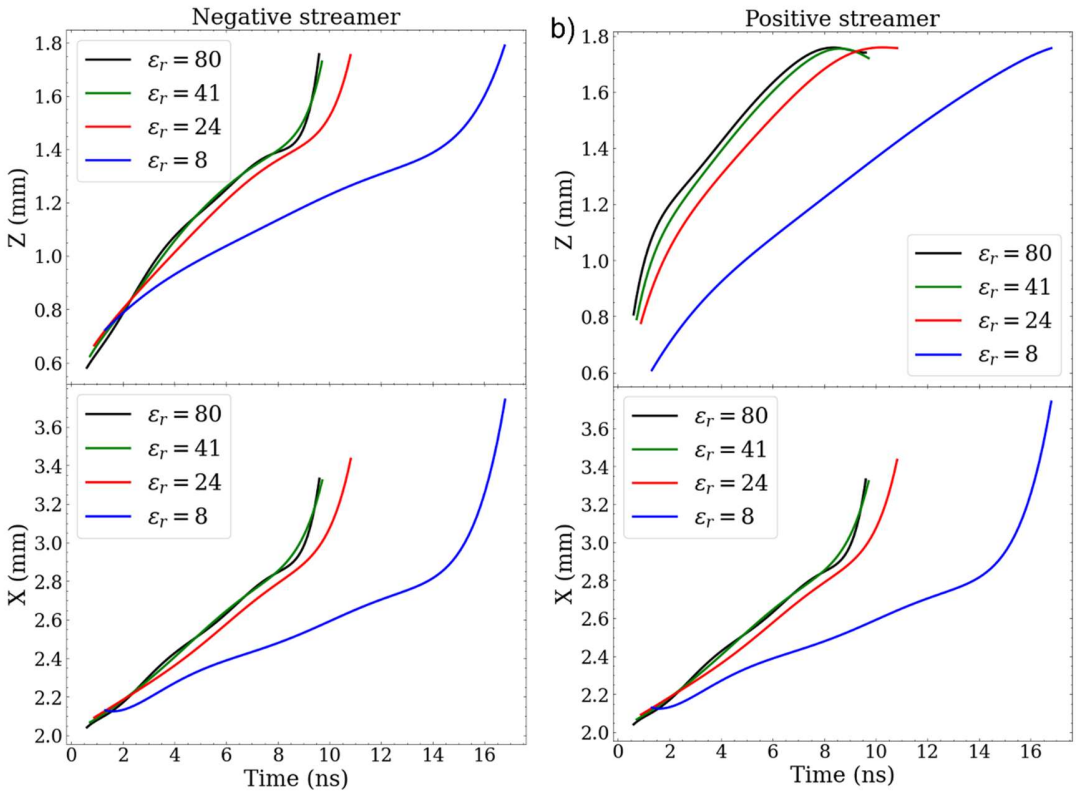

Figure 7: *Time evolution of the positions, X and Z, of a) the negative and b) positive streamers' head propagating in air gap with a droplet that has different dielectric permittivity, namely 8, 24, 41, and 80.*

It can be easily concluded that the dielectric property of the droplet has a strong influence on the behavior of positive and negative streamers in the gap. Indeed, streamer dynamic is strongly coupled to electric field distribution. Therefore, a modification of its spatial distribution, due to normal electric field component enhancement at the surface of the droplet, can lead to a variation of streamers' velocities and electron density in the conductive channel.

4.3 Effect of the wetting angle

In this section, the droplet shape is modified to consider different wetting angle (θ) between Teflon and a droplet with a dielectric permittivity of 80. The influence of θ on discharge ignition and propagation is of interest as it can be encountered in several experimental configurations, such as water droplets at high voltage lines. θ is defined as the angle formed by the Teflon's surface and the droplet's surface, as presented in Figure 8. Three typical cases are considered in the study: 90°, 112° (hydrophilic behavior), and 22° (hydrophobic behavior).

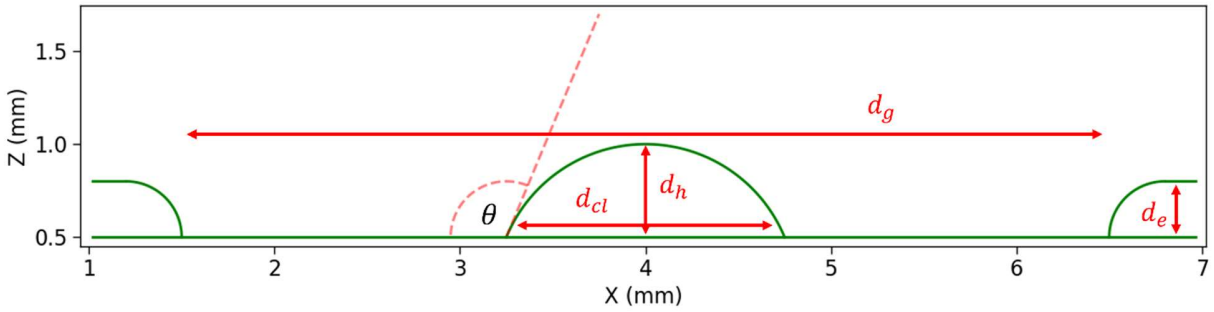

Figure 8: *Scheme of the configuration to model the influence of the wetting angle between the droplet and Teflon. The parameters are fixed to d_e = 0.3 mm, d_g = 5 mm, d_{cl} = 1.5 mm, and d_h can change with θ; three values are considered: 22, 90, and 112°.*

Figure 9 shows the temporal evolution of the electron density for each case of θ. The propagation of both positive and negative streamers is influenced by θ. In the case of $\theta = 90$ ° (Figure 9a), a plasma channel connects the anode to the droplet and a propagation along the droplet's surface is also visible (at 10.4 ns). At 12.8 ns, the propagation of the positive streamer on the droplet's surface continues, in addition to the presence of plasma channel between the cathode and the droplet. At 14.3 ns, both negative and positive streamers continue to propagate at the droplet's surface and, at 15.5ns, a connection between the two streamers is occurred. In the last image (at 15.5 ns), the

551 bump due to the connection of the two streamers is clearly visible and is localized almost at the
552 top of the droplet. In the case of $\theta = 112°$ (Figure 9b), the propagation steps are rather similar to
553 the previous one with few differences, mainly the lower electron density in the channel propagation
554 above Teflon and the displacement of the bump towards the anode (it remains on the droplet's
555 surface) due to a larger delay before the ignition of the positive streamer propagation (time needed
556 to produce enough space charge to deform the electric field). Compared to the previous case, the
557 bumps produced in this case ($\theta = 112°$) appears larger. In the case of $\theta = 22°$ (Figure 9c), the
558 plasma channel connects the anode to the droplet equator, and propagation in two directions are
559 observed: towards Teflon and towards droplet's top. Similar propagation is observed from the
560 cathode side. This propagation seems to be delayed by few nanoseconds as compared to the
561 positive one (Figure 9c at 3.7 ns), however this behavior is due to the low electron density in the
562 plasma channel. The electric field, presented in Figure 10c at 3.7 ns, demonstrates the presence of
563 the negative streamer on the dielectric surface at the same time than the positive one. The last
564 image at 9.7 ns shows the connection between the two streamers and the formation of the bump
565 which is shifted towards the cathode.

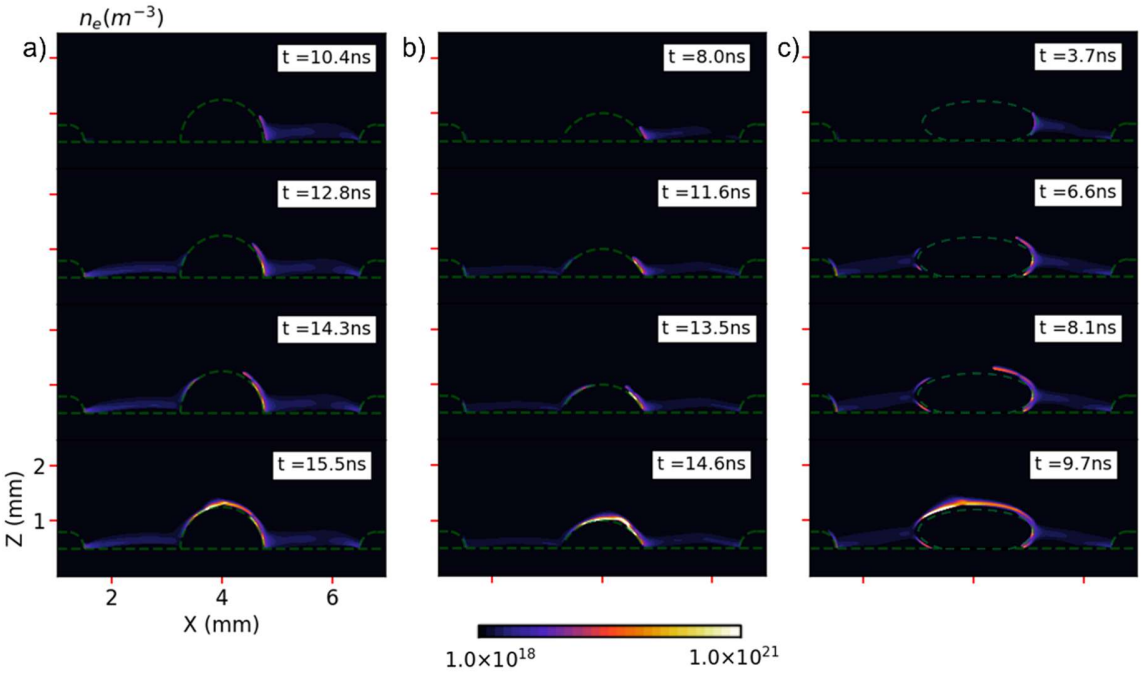

Figure 9: *Time evolution of electron density for streamer discharges propagating in air gap with a droplet that has different contact angle with Teflon, namely a) 90°, b) 112°, and c) 22°.*

The streamer propagation paths described earlier for the different θ-conditions can be well explained by the electric field. The temporal evolution of the electric field distribution is shown in Figure 10 for each case of θ. In the case of $\theta = 90°$ and 112°, the electric field is amplified in the area near the intersection of air-Teflon-droplet. Therefore, both streamers touch the droplet near the Teflon surface, as shown in Figures 10a and 10b. In the two previous cases, the global dynamic of both streamers is similar. However, the droplet in the case of $\theta = 90°$ exhibits a height relatively larger than the case of $\theta = 112°$, which makes the major movement along the Z axis and, thus, the contact point between positive and negative streamers is established later. In the case of $\theta = 22°$, the shape of the droplet induced an electric field amplification on the droplet's equator, where the curvature radius is small. Positive and negative streamers are attracted by this area of high electric field.

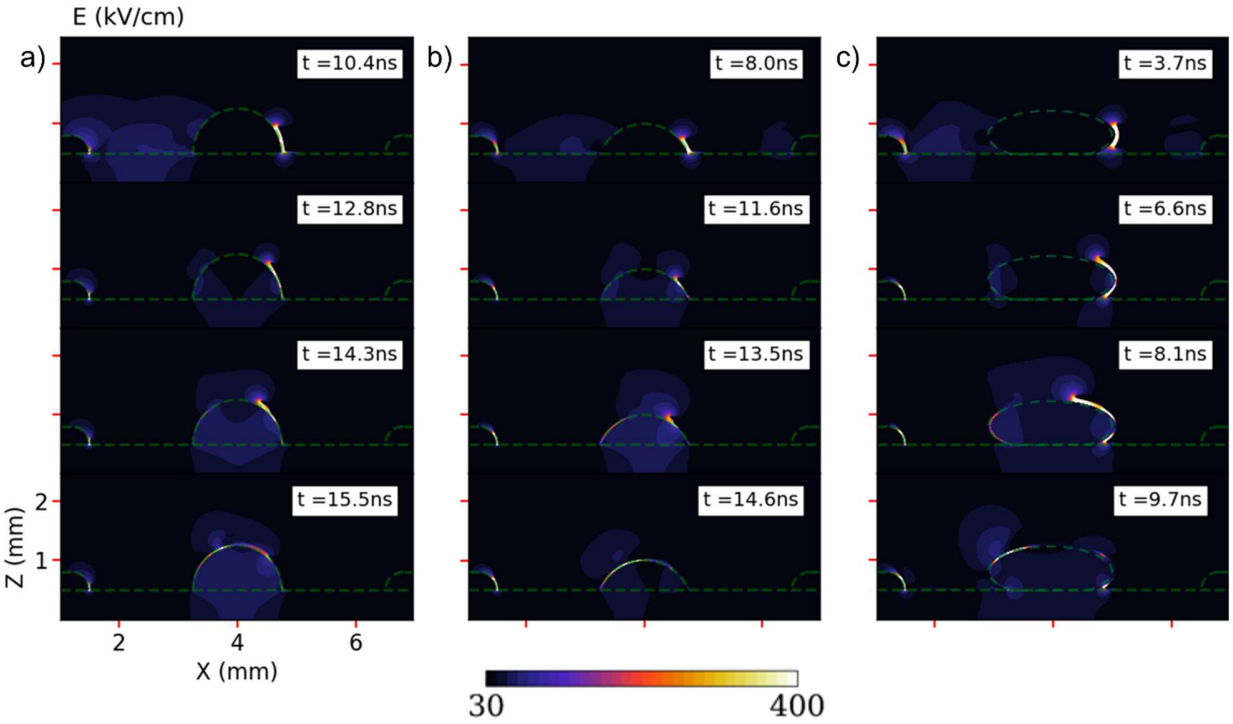

Figure 10: *Time evolution of electric field for streamer discharges propagating in air gap with a droplet that has different contact angle with Teflon, namely a) 90°, b) 112°, and c) 22°.*

The modification of θ strongly modifies the shape of the droplet and, thus, the electric field distribution. Therefore, the dynamics of both positive and negative streamers is impacted. It is also interesting to note that discharge properties (electron density, velocities, path) are sensitive to the shape of the dielectric surface. This last point is of interest and deserves further investigation.

5. CONCLUSION

In this paper, we developed a 2D numerical model to study the spatial-temporal evolution of a streamer discharge in air, between two pins where a droplet of deionized water is lying on Teflon surface. Streamers propagated relatively quickly (around 10 nanoseconds), which allowed us to consider the water droplet as perfect dielectric with a permittivity of 80. The model consisted of resolving Poisson's equation together with the drift-diffusion equation for electrons, positive ions,

and negative ions. Photoionization was also considered in the model thanks to Helmholtz equations. The model results, particularly the electron impact source ionization (S_e), was compared with discharge emission captured by 1 ns-exposure ICCD camera. Such a comparison allowed a validation of the model. In general, the discharge is ignited at both electrodes and positive and negative streamers propagated towards the droplet. The positive streamer starts its propagation after the negative streamer due to the time needed to generate enough space charge to deform the applied electric field. Then, they propagated at the droplet surface with velocities that depend on their location on the droplet as well as on the distance separating their heads. The model allowed us to address the contact point of the two streamers with high resolution, spatially and temporally. Indeed, when the streamers approached each other, the distribution of the electric field is strongly modified/enhanced locally, leading to an acceleration and peeling of the negative streamer from the droplet's surface; a bump is thus observed. On the other hand, the influence of the dielectric permittivity and wetting angle of the droplet on the discharge were investigated. We found that these two parameters strongly influenced the electric field distribution and, therefore, the propagation paths and the properties of both positive and negative streamers. For instance, the increase of the dielectric permittivity has led to an increase of the propagation velocity and of the electron density in the conductive channel. The findings reported here are of interest for many applications that employ the processing of various droplet with different geometries.

DATA AVAILABILITY statement

All data that support the findings of this study are included within the article (and any supplementary files).

ACKNOWLEDGEMENT

The research reported in this publication was financially supported by the Natural Sciences and Engineering Research Council of Canada (NSERC), under award number RGPIN-2023-03951.

Conflict of Interest

The authors have no conflicts to disclose.

ORCID iDs

Lyes Sebih · https://orcid.org/0000-0001-7832-1478

Flavien Valensi · https://orcid.org/0000-0002-2211-4995

Ahmad Hamdan · https://orcid.org/0000-0001-5591-2291

REFERENCES:

[1] S. Nijdam, J. Teunissen, et U. Ebert, « The physics of streamer discharge phenomena », *Plasma Sources Sci. Technol.*, vol. 29, nº 10, p. 103001, nov. 2020, doi: 10.1088/1361-6595/abaa05.

[2] E. M. V. Veldhuizen et W. R. Rutgers, « Pulsed positive corona streamer propagation and branching », *J. Phys. Appl. Phys.*, vol. 35, nº 17, p. 2169-2179, sept. 2002, doi: 10.1088/0022-3727/35/17/313.

[3] A. Mizuno, « Industrial applications of atmospheric non-thermal plasma in environmental remediation », *Plasma Phys. Control. Fusion*, vol. 49, nº 5A, p. A1-A15, mai 2007, doi: 10.1088/0741-3335/49/5A/S01.

[4] O. V. Penkov, M. Khadem, W.-S. Lim, et D.-E. Kim, « A review of recent applications of atmospheric pressure plasma jets for materials processing », *J. Coat. Technol. Res.*, vol. 12, nº 2, p. 225-235, mars 2015, doi: 10.1007/s11998-014-9638-z.

[5] G. Fridman, G. Friedman, A. Gutsol, A. B. Shekhter, V. N. Vasilets, et A. Fridman, « Applied Plasma Medicine », *Plasma Process. Polym.*, vol. 5, nº 6, p. 503-533, 2008, doi: 10.1002/ppap.200700154.

[6] A. Abou-Ghazala, S. Katsuki, K. H. Schoenbach, F. C. Dobbs, et K. R. Moreira, « Bacterial decontamination of water by means of pulsed-corona discharges », *IEEE Trans. Plasma Sci.*, vol. 30, nº 4, p. 1449-1453, août 2002, doi: 10.1109/TPS.2002.804193.

[7] P. Laroche, P. Blanchet, A. Delannoy, et F. Issac, « Experimental Studies of Lightning Strikes to Aircraft », nº 5, 2012.

[8] P. Vanraes et A. Bogaerts, « The essential role of the plasma sheath in plasma–liquid interaction and its applications—A perspective », *J. Appl. Phys.*, vol. 129, nº 22, p. 220901, juin 2021, doi: 10.1063/5.0044905.

[9] J. Diamond, A. Hamdan, J. Profili, et J. Margot, « Time and space-resolved imaging of an AC air discharge in contact with water », *J. Phys. Appl. Phys.*, vol. 53, nº 42, p. 425209, oct. 2020, doi: 10.1088/1361-6463/ab9f69.

[10] Liu J and Hu X 2013 « Contrasting Behaviours of AC and DC Excited Plasmas in Contact with Liquid », *Plasma Sci. Technol.*, vol. 15, nº 8, p. 768, août 2013, doi: 10.1088/1009-0630/15/8/10.

[11] Y. E. Kovach, M. C. Garcia, et J. E. Foster, « The variation in self-organized anode plasma pattern structure with solution electrolyte type in 1 atm DC glow discharge », *Plasma Sources Sci. Technol.*, vol. 30, nº 1, p. 015007, janv. 2021, doi: 10.1088/1361-6595/abc815.

[12] Y. CHEN, B. FENG, Q. ZHANG, R. WANG, K. (Ken) OSTRIKOV, et X. ZHONG, « Temperature dependence of pattern transitions on water surface in contact with DC microplasmas », *Plasma Sci. Technol.*, vol. 22, nº 5, p. 055404, févr. 2020, doi: 10.1088/2058-6272/ab66e9.

[13] X. Li, S. Zhou, K. Gao, J. Ran, K. Wu, et P. Jia, « Temporal Evolutions of Self-Organized Patterns Formed on the Water-Anode Surface of an Atmospheric Pressure Glow Discharge », *IEEE Trans. Plasma Sci.*, vol. 50, nº 6, p. 1717-1722, 2022, doi: 10.1109/TPS.2022.3156027.

[14] A. Herrmann, J. Margot, et A. Hamdan, « Influence of voltage and gap distance on the dynamics of the ionization front, plasma dots, produced by nanosecond pulsed discharges at water surface », *Plasma Sources Sci. Technol.*, vol. 31, nº 4, p. 045006, avr. 2022, doi: 10.1088/1361-6595/ac5ec8.

[15] I. Adamovich *et al.*, « The 2022 Plasma Roadmap: low temperature plasma science and technology », *J. Phys. Appl. Phys.*, vol. 55, nº 37, p. 373001, sept. 2022, doi: 10.1088/1361-6463/ac5e1c.
[16] S. Coquillat, « Corona emission from raindrops in strong electric fields as a possible discharge initiation: Comparison between horizontal and vertical field configurations », *J. Geophys. Res.*, vol. 108, nº D7, p. 4205, 2003, doi: 10.1029/2002JD002714.
[17] J. Menneveux et J. Veilleux, « Optical Emission Spectroscopy Study of Plasma-Precursor Interactions in TiO2 Suspension Plasma Spray », *Plasma Chem. Plasma Process.*, vol. 42, mai 2022, doi: 10.1007/s11090-022-10236-4.
[18] G. Oinuma, G. Nayak, Y. Du, et P. J. Bruggeman, « Controlled plasma–droplet interactions: a quantitative study of OH transfer in plasma–liquid interaction », *Plasma Sources Sci. Technol.*, vol. 29, nº 9, p. 095002, sept. 2020, doi: 10.1088/1361-6595/aba988.
[19] Z. Zhao *et al.*, « The dynamic evolution of atmospheric-pressure pulsed air discharge over a water droplet », *Phys. Plasmas*, vol. 29, nº 4, p. 043507, avr. 2022, doi: 10.1063/5.0083246.
[20] A. Hamdan et A. Dorval, « Spatial and temporal dynamics of single nanosecond discharges in air with water droplets », *J. Phys. Appl. Phys.*, vol. 56, nº 21, p. 215202, mai 2023, doi: 10.1088/1361-6463/acc53e.
[21] N. Y. Babaeva et M. J. Kushner, « Effect of inhomogeneities on streamer propagation: I. Intersection with isolated bubbles and particles », *Plasma Sources Sci. Technol.*, vol. 18, nº 3, p. 035009, août 2009, doi: 10.1088/0963-0252/18/3/035009.
[22] N. Y. Babaeva et M. J. Kushner, « Effect of inhomogeneities on streamer propagation: II. Streamer dynamics in high pressure humid air with bubbles », *Plasma Sources Sci. Technol.*, vol. 18, nº 3, p. 035010, août 2009, doi: 10.1088/0963-0252/18/3/035010.
[23] N. Y. Babaeva et M. J. Kushner, « Structure of positive streamers inside gaseous bubbles immersed in liquids », *J. Phys. Appl. Phys.*, vol. 42, nº 13, p. 132003, juill. 2009, doi: 10.1088/0022-3727/42/13/132003.
[24] K. Konina, J. Kruszelnicki, M. E. Meyer, et M. J. Kushner, « Surface ionization waves propagating over non-planar substrates: wavy surfaces, cut-pores and droplets », *Plasma Sources Sci. Technol.*, vol. 31, nº 11, p. 115001, nov. 2022, doi: 10.1088/1361-6595/ac9a6c.
[25] Herrmann A, Margot J and Hamdan A 2024 Experimental and 2D fluid simulation of a streamer discharge in air over a water surface Plasma Sources Sci. Technol. **33** 025022
[26] J. Teunissen, « Improvements for drift-diffusion plasma fluid models with explicit time integration », *Plasma Sources Sci. Technol.*, vol. 29, nº 1, p. 015010, janv. 2020, doi: 10.1088/1361-6595/ab6757.
[27] M. Arrayas, M. A. Fontelos, et J. L. Trueba, « Photoionization effects in streamer discharges », p. 18.
[28] B. Bagheri *et al.*, « Comparison of six simulation codes for positive streamers in air », *Plasma Sources Sci. Technol.*, vol. 27, nº 9, p. 095002, sept. 2018, doi: 10.1088/1361-6595/aad768.
[29] M. B. Zhelezniak, A. Kh. Mnatsakanian, et S. V. Sizykh, « Photoionization of nitrogen and oxygen mixtures by radiation from a gas discharge », *High Temp. Sci.*, vol. 20, p. 357-362, nov. 1982.
[30] S. Celestin, « Study of the dynamics of streamers in air at atmospheric pressure », p. 197.
[31] A. Luque, U. Ebert, C. Montijn, et W. Hundsdorfer, « Photoionization in negative streamers: Fast computations and two propagation modes », *Appl. Phys. Lett.*, vol. 90, nº 8, p. 081501, févr. 2007, doi: 10.1063/1.2435934.

[32] A. A. Dubinova, *Modeling of streamer discharges near dielectrics*. Eindhoven: TU Eindhoven, 2016.
[33] J. Kruszelnicki, A. M. Lietz, et M. J. Kushner, « Atmospheric pressure plasma activation of water droplets », *J. Phys. Appl. Phys.*, vol. 52, nº 35, p. 355207, août 2019, doi: 10.1088/1361-6463/ab25dc.
[34] J. W. Demmel, N. J. Higham, et R. S. Schreiber, « Stability of blockLU factorization », *Numer. Linear Algebra Appl.*, vol. 2, nº 2, p. 173-190, mars 1995, doi: 10.1002/nla.1680020208.
[35] P. Virtanen *et al.*, « SciPy 1.0: fundamental algorithms for scientific computing in Python », *Nat. Methods*, vol. 17, nº 3, p. 261-272, mars 2020, doi: 10.1038/s41592-019-0686-2.
[36] P. Tamamidis, « A new upwind scheme on triangular meshes using the finite volume method », *Comput. Methods Appl. Mech. Eng.*, vol. 124, nº 1-2, p. 15-31, juin 1995, doi: 10.1016/0045-7825(94)00751-8.
[37] D. Zhang, C. Jiang, D. Liang, et L. Cheng, « A review on TVD schemes and a refined flux-limiter for steady-state calculations », *J. Comput. Phys.*, vol. 302, p. 114-154, déc. 2015, doi: 10.1016/j.jcp.2015.08.042.
[38] S. V. Patankar, *Numerical heat transfer and fluid flow*. in Series in computational methods in mechanics and thermal sciences. Boca Raton: CRC Press, 2009.
[39] A. A. Kulikovsky, « A More Accurate Scharfetter-Gummel Algorithm of Electron Transport for Semiconductor and Gas Discharge Simulation », *J. Comput. Phys.*, vol. 119, nº 1, p. 149-155, juin 1995, doi: 10.1006/jcph.1995.1123.
[40] H. J. Teunissen, « 3D Simulations and Analysis of Pulsed Discharges », p. 219.
[41] C. Montijn, W. Hundsdorfer, et U. Ebert, « An adaptive grid refinement strategy for the simulation of negative streamers », *J. Comput. Phys.*, vol. 219, nº 2, p. 801-835, déc. 2006, doi: 10.1016/j.jcp.2006.04.017.
[42] J. Teunissen et U. Ebert, « Simulating streamer discharges in 3D with the parallel adaptive Afivo framework », *J. Phys. Appl. Phys.*, vol. 50, nº 47, p. 474001, nov. 2017, doi: 10.1088/1361-6463/aa8faf.
[43] J.-P. Boeuf, L. L. Yang, et L. C. Pitchford, « Dynamics of a guided streamer ('plasma bullet') in a helium jet in air at atmospheric pressure », *J. Phys. Appl. Phys.*, vol. 46, nº 1, p. 015201, janv. 2013, doi: 10.1088/0022-3727/46/1/015201.
[44] Q. Zhang, L. Zhang, D. Yang, J. Schulze, Y. Wang, et A. Bogaerts, « Positive and negative streamer propagation in volume dielectric barrier discharges with planar and porous electrodes », *Plasma Process. Polym.*, vol. 18, nº 4, p. 2000234, avr. 2021, doi: 10.1002/ppap.202000234.
[45] X. Chen, Y. Zhu, et Y. Wu, « Modeling of streamer-to-spark transitions in the first pulse and the post discharge stage », *Plasma Sources Sci. Technol.*, vol. 29, nº 9, p. 095006, sept. 2020, doi: 10.1088/1361-6595/ab8e4e.